Research Square

Preprints are preliminary reports that have not undergone peer review.
They should not be considered conclusive, used to inform clinical practice,
or referenced by the media as validated information.

Enhancement of machining quality in electrochemical mill-grinding of titanium matrix composites utilizing a follow-up auxiliary anode

Shen Niu

ns2019@hpu.edu.cn

Henan Polytechnic University

Yansen Peng
Pingmei Ming
Kaiqiang Huang
Shijie Fan
Wenjie Liu
Lei Ren

Research Article

Keywords: electrochemical mill-grinding, titanium matrix composites, auxiliary anode, surface flatness, surface roughness

Posted Date: June 11th, 2026

DOI: https://doi.org/10.21203/rs.3.rs-9567525/v1

License: This work is licensed under a Creative Commons Attribution 4.0 International License.
Read Full License

Version of Record: A version of this preprint was published at The International Journal of Advanced Manufacturing Technology on July 27th, 2026. See the published version at https://doi.org/10.1007/s00170-026-18830-y.

Enhancement of machining quality in electrochemical mill-grinding of titanium matrix composites utilizing a follow-up auxiliary anode

Shen Niu [a, b, *], Yansen Peng [a], Pingmei Ming [a, b], Kaiqiang Huang [a], Shijie Fan [a], Wenjie Liu [a, b], Lei Ren [a]

[a] School of Mechanical and Power Engineering, Henan Polytechnic University, Jiaozuo 454003 China

[b] Henan International Joint Laboratory of Advanced Electronic Packaging Materials Precision Forming, Henan Polytechnic University, Jiaozuo 454003, China

* Corresponding author. E-mail address: ns2019@hpu.edu.cn

Abstract

Electrochemical mill-grinding (ECMG) has the potential to be used for successive rough and finish machining of titanium matrix composites. However, severe stray corrosion occurs on the machined surface during the rough machining stage, leading to prolonged machining time in the subsequent finish machining stage. In this study, follow-up auxiliary anode electrochemical mill-grinding (FAAECMG) was innovatively proposed for enhancing the machining quality of titanium matrix composites. Dynamic electric field simulation showed that introducing the auxiliary anode with a positive potentially difference radically altered the current direction in the machined area, which significantly improved process localization. Experimental results verified that, compared with traditional ECMG, the surface flatness decreased from 322.25 μm to 152.44 μm and the surface roughness reduced from 16.76 μm to 11.84 μm when FAAECMG with a positive potential difference of 15 V was used. Compared with rough machining, the surface flatness decreased from 152.44 μm to 5.368 μm, the surface roughness reduced from 11.84 μm to 0.669 μm, and the surface residual compressive stress increased from -116.07 MPa to -407.94 MPa after finish machining. Therefore, the newly proposed method offers advantages in improving machining accuracy and surface quality in ECMG and reducing the machining cycle of components.

Keywords: electrochemical mill-grinding; titanium matrix composites; auxiliary anode; surface flatness; surface roughness.

1. Introduction

Titanium matrix composites are widely used in aerospace because of their unique properties, including a high strength-to-weight ratio, excellent fatigue strength, and exceptional corrosion resistance [1,2]. However, titanium matrix composites is well known as a difficult-to-cut material, posing a challenge for traditional cutting processes due to significant tool wear, poor surface quality, and high residual stress [3,4]. Stepped structures are common features in machinery design and are often used for fixing and supporting components in assemblies. They are also typical structural characteristics of integral aerospace components [5]. Therefore, achieving high efficiency, excellent precision, and good surface integrity in the machining of stepped structures made of titanium matrix composites remains a significant challenge and an important research focus in aerospace.

Electrochemical mill-grinding (ECMG) is a hybrid machining pattern that combines electrochemical anodic dissolution and mechanical grinding, using a rod-shaped electrode embedded with abrasive particles [6,7,8]. ECMG combines electrochemical (EC) milling and electrochemical grinding (ECG) in a single processing procedure. Therefore, rough and finish machining operations in ECMG can be combined without the need to replace the tool and re-fixture the workpiece. During the rough machining stage, ECMG operates similarly to EC milling, and its main goal is to achieve a high MRR and no tool wear [8,9]. During the finish machining stage, ECMG operates similarly to ECG, and its primary purpose is to obtain high machining accuracy with good surface quality [8,10]. As a result, ECMG demonstrates significant application potential for the rough and finish machining of complex components made from titanium matrix composites.

According to the mode of electrolyte supply, ECMG can be divided into two categories, is also named as inner-jet ECMG and outer-jet ECMG [7]. In inner-jet ECMG, the abrasive tool is a rotating electrode with a dead-end tube that machines the side wall of the workpiece at a required depth of cut. The electrolyte is sprayed onto the machining surface through outlets located on the side wall of the abrasive tool. Inner-jet ECMG allows for efficient removal of a large machining allowance in a single pass

[8,11,12,13]. However, the design of the outlet geometry, number, and layout, as well as the manufacturing of abrasive tools with side-wall outlets, requires considerable time and cost. In outer-jet ECMG, the abrasive tool is a rotating electrode with a solid rod-shaped structure, and the electrolyte is sprayed toward the machining region from the external nozzle [14,15,16]. This configuration eliminates the complex design and manufacturing processes associated with inner-jet abrasive tools, thereby significantly reducing time and cost. Moreover, outer-jet ECMG is primarily applied under a one-sided constraint condition, in which either the left or right side of the tool is covered by the workpiece. Because a stepped structure consists of a flat surface and a side wall, only one side of the abrasive tool is constrained by the workpiece during ECMG. Therefore, outer-jet ECMG is more suitable for processing stepped structures made of difficult-to-cut materials.

Niu et al. [16] achieved rough and finish machining of a (TiB+TiC)Ti-6Al-4V stepped structure using outer-jet ECMG with the same tool and electrolyte. However, regardless of whether inner-jet ECMG or outer-jet ECMG is employed, a substantial flow of electrolyte inevitably remains on the machined surface of the workpiece. Because a high voltage is applied during the rough machining stage of ECMG, severe stray corrosion occurs on the machined surface, resulting in poor machining accuracy and consequently a prolonged finish machining stage. It should be noted that when a specially designed auxiliary anode with a higher potential than that of the workpiece is introduced into electrochemical machining, the electric field distribution in the machined area can be altered, thereby effectively suppressing stray corrosion on the machined surface. Therefore, the machining accuracy can be effectively improved compared with traditional electrochemical machining. Zhu et al. [17] proposed a sleeve-shaped auxiliary anode positioned above the cathode and applied a positive potential difference between the auxiliary anode and the workpiece, which caused more power lines to concentrate on the auxiliary anode, thereby effectively protecting the machined area. As a result, the machining accuracy of electrochemical trepanning of Ti-6Al-4V blades was improved. Zhang et al. [18] designed a trapezoidal auxiliary anode mounted on the side of the tool, which significantly reduced the taper of Inconel 718 blades

during conventional electrochemical machining. Therefore, incorporating a specially designed auxiliary anode during the rough machining stage of ECMG has the potential to enhance process localization and effectively shorten the subsequent finish machining stage. Unfortunately, there have been no reports that discuss the development and application of auxiliary anode in ECMG.

In this study, follow-up auxiliary anode electrochemical mill-grinding (FAAECMG) is innovatively proposed to improve machining accuracy and surface quality during the rough machining of titanium matrix composites. First, an auxiliary anode with a curved surface and a corresponding follow-up conductive device are designed and manufactured. Second, the mechanism by which stray corrosion on the machined surface is suppressed using FAAECMG is clarified through dynamic electric field simulation. Subsequently, the reliability of the simulation results and the feasibility of the innovatively proposed method are verified through experimental investigations. Finally, a titanium matrix composites stepped structure with high machining accuracy and good surface integrity is fabricated using ECMG by combining the rough and finish machining.

2. Description of the method

Fig. 1 shows a schematic illustration of the FAAECMG. As shown in the figure, the cathode tool has a rod-shaped structure, with abrasive grains distributed on the end face and side wall of the tool within a specified region. An auxiliary anode with a cuboid structure and a curved surface on one side was designed and installed behind the abrasive tool along the feed direction. The circumferential surface of the abrasive tool was coaxially aligned with the curved surface of the auxiliary anode, and the end face of the tool was coplanar with that of the auxiliary anode. During the machining process, the abrasive tool rotated at a high-speed while being fed along a predefined path at a specified feed rate. The auxiliary anode followed the abrasive tool along the same path and at the same feed rate. The abrasive tool was connected to the negative terminal of the power supply, while both the auxiliary anode and the anode workpiece were connected to the positive terminal. An electronic load was connected between the positive terminal of the power supply and the anode workpiece. By adjusting the circuit

resistance through the electronic load, the potential of the auxiliary anode was maintained higher than that of the anode workpiece, thereby establishing a stable positive potential difference between them. According to classical electric field theory, electric current flows from equipotential surfaces at a higher potential to those at a lower potential, and the electrochemical dissolution occurs at electrodes with a higher potential [19]. Although the auxiliary anode has the highest potential, electrochemical dissolution does not occur on its surface because it is coated with an inert metal layer. Compared with conventional ECMG, the proposed method effectively suppresses stray corrosion on the machined surface, thereby enhancing the machining quality of anode workpiece.

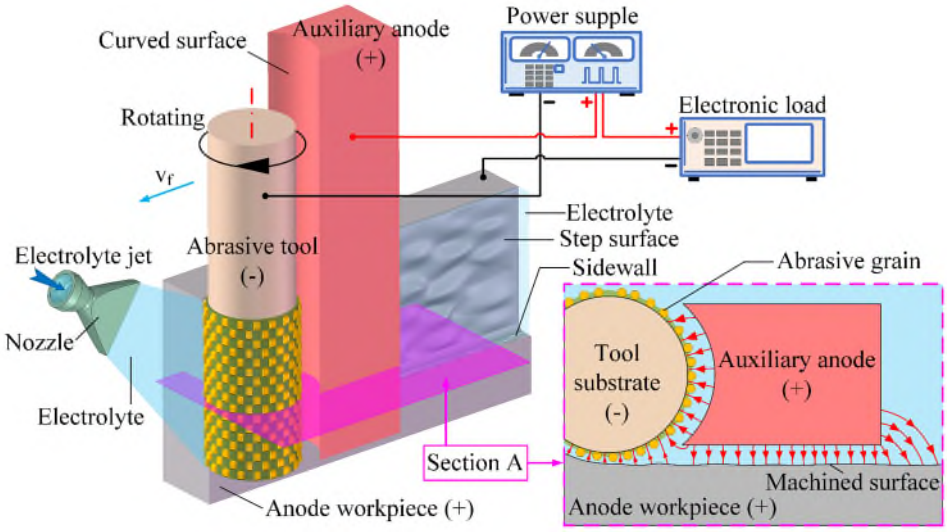


Fig. 1 Schematic illustration of the FAAECMG.

The structural design of the working part of the auxiliary anode is illustrated in Fig. 2 R_1 denotes the radius of the curved surface of the auxiliary anode, while L_1, L_2, and L_3 represent the width, height, and length of the working part, respectively. D denotes the diameter of the tool substrate, and H represents the height of the abrasive layer. C denotes the normal gap between the curved surface of the auxiliary anode and the side wall of the tool substrate. A smaller value of C enhances the ability of the auxiliary anode to absorb the stray electric field in the machined area. However, an excessively small C may lead to spark discharge between the auxiliary anode and the abrasive tool due to the large potential difference between them. Similarly, increasing L_1 improves the absorption of the stray electric field, whereas an excessively larger L_1

may cause interference between the auxiliary anode and the anode workpiece. In addition, to ensure complete coverage of the machined step surface, L_2 should not be too small. To maintain adequate structural rigidity of the auxiliary anode, L_3 should also not be too small. Based on this analysis, the structural dimensions of the auxiliary anode should satisfy the following relationships:

$$R_1=D/2+C \tag{1}$$

$$L_1<D \tag{2}$$

$$L_2>H \tag{3}$$

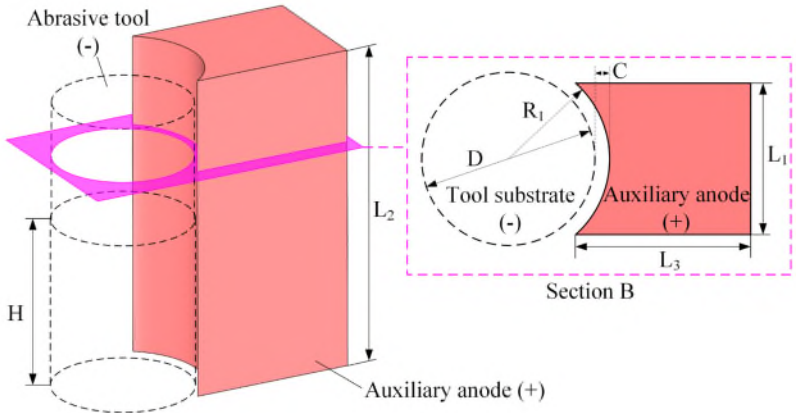


Fig. 2 Structural design of the working part of the auxiliary anode.

3. Numerical simulation model

In this study, based on the machining requirements for the stepped structure of titanium matrix composites, the diameter of the tool substrate D was set to 6 mm, and the height of the abrasive layer H was 8 mm. The normal gap *C* between the curved surface of the auxiliary anode and the side wall of the tool substrate was set to 0.5 mm. Accordingly, the radius of the curved surface of the auxiliary anode, R_1, was calculated as 3.5 mm, based on the above equations. The width L_1, height L_2, and length L_3 of the working part of the auxiliary anode were set to 5.6 mm, 14 mm, and 7 mm, respectively.

To elucidate the mechanism by which the proposed method suppresses stray corrosion on the machined surface, an electric field simulation was conducted. To simplify the physical model, the abrasive particles on the tool were neglected, thereby reducing computational complexity. The initial machining gap between the cathode tool and the anode workpiece was set to 0.2 mm. The depth of cut for a single tool pass was

set to 0.1 mm. An electric field simulation model was established, as shown in Fig. 3, and the following conditions and assumptions were adopted:

(1) The electrolyte conductivity remains approximately constant.

(2) The surfaces of the cathode and anode are treated as equipotential surfaces.

(3) The electrolyte is considered to be isotropic, with constant electrical conductivity.

Based on the above assumptions, the electric potential φ in the computational domain is governed by the Laplace equation [20,21]:

$$\nabla^2\varphi=0 \tag{4}$$

For conventional ECMG, the boundary conditions are defined as

$$\varphi|\Gamma_1=0 \text{ (tool)} \tag{5}$$

$$\varphi|\Gamma_{2,3}=U \text{ (workpiece)} \tag{6}$$

$$\frac{\partial\varphi}{\partial n}|\Gamma_{4,5,6,7}=0 \text{ (other boundaries)} \tag{7}$$

For FAAECMG, the boundary conditions are defined as

$$\varphi|\Gamma_1=0 \text{ (tool)} \tag{8}$$

$$\varphi|\Gamma_{2,3,4,5}=U_1 \text{ (auxiliary anode)} \tag{9}$$

$$\varphi|\Gamma_{6,7}=U \text{ (workpiece)} \tag{10}$$

$$\frac{\partial\varphi}{\partial n}|\Gamma_{8,9,10,11}=0 \text{ (other boundaries)} \tag{11}$$

where U is the applied voltage, U_1 is the voltage of the auxiliary anode, and n is the normal vector of the surface.

Based on the above electric field model and its corresponding boundary conditions, electric field simulations were conducted using COMSOL. In the simulations, the feed rate of the tool was set to 7 mm/min, the electrolyte conductivity K was 10 S/m, and the potential U of the anode workpiece was 25 V. The auxiliary anode potential U_1 was set to 30 V, 35 V, 40 V, 45 V, and 50 V. Accordingly, the positive potential difference ΔU between the auxiliary anode and the anode workpiece was calculated using Eq. (12) and set to 5 V, 10 V, 15 V, 20 V, and 25 V, respectively.

$$\Delta U = U_1 - U \tag{12}$$

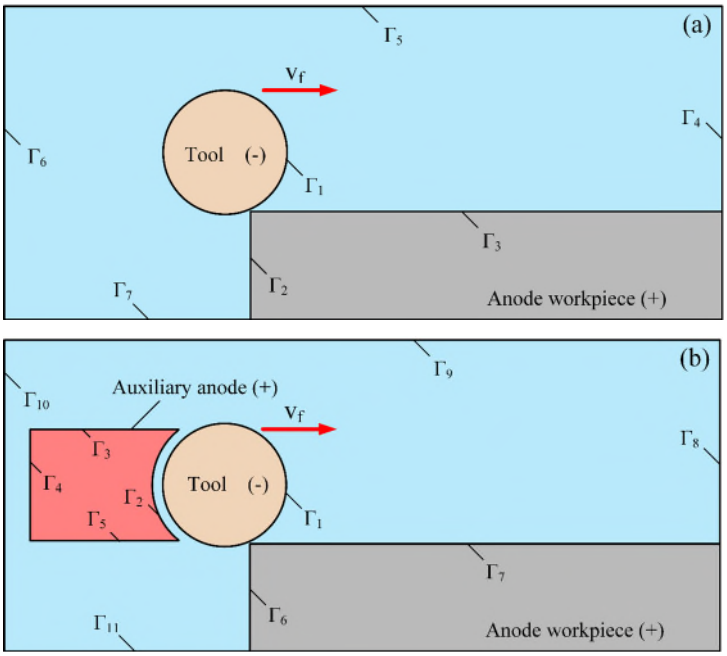


Fig. 3 Physical model for electric field simulation: (a) Traditional ECMG, (b) FAAECMG.

4. Design of the experimental system

The precision electrochemical mill-grinding machine has been reported in previous research [22]. As shown in Fig. 4, a specially designed follow-up conductive device, referred to as Unit A, was manufactured and installed on the motor spindle. Unit A consists of an insulating mounting plate, an insulating mounting block, an insulating slide block, a conductive bolt, and an adjusting bolt. The adjusting bolt is screwed into a threaded hole in the insulating mounting block, and its end is connected to the insulating slide block by a fixing pin. The auxiliary anode is mounted on the insulating slide block using connection bolts and is connected to the positive terminal of the power supply through the conductive bolt. The position of the auxiliary anode can be adjusted along the Z-axis via the adjustment bolt. Unit A is fixed onto the clamping seat using the insulating mounting plate, ensuring that the auxiliary anode follows the abrasive tool at the same feed rate during machining. Units B and C are the revolving conductive device of the tool and the fixture of the workpiece, respectively. Their structures and principles are consistent with those described in the literature [20]. In FAAECMG, the auxiliary anode is electrically connected to Unit A, while the tool and the workpiece are connected to Units B and C, respectively. Units A and B are connected to the positive

and negative terminals of the power supply, respectively, whereas Unit C is connected to one terminal of the electronic load, with the other terminal of the electronic load connected to the positive terminal of the power supply. In conventional ECMG, the tool cathode is energized through Unit B, while the workpiece is connected directly to the positive terminal of the power supply through Unit C.

Fig. 5 shows a photograph of the auxiliary anode and its conductive device. The substrate of the auxiliary anode was fabricated from TA1 titanium, and an iridium–tantalum alloy coating was applied on its surface. The abrasive tool was embedded with diamond abrasive grains with a grit size of 270/325. The workpiece material is (TiB+TiC)/Ti-6Al-4V, which is a one of the most commonly used titanium matrix composites in aerospace. The proportions of the reinforcing phase and matrix listed in Table 1. The electrolyte was a $NaNO_3$ solution with a mass fraction of 10%, maintained at a temperature of 30 °C.

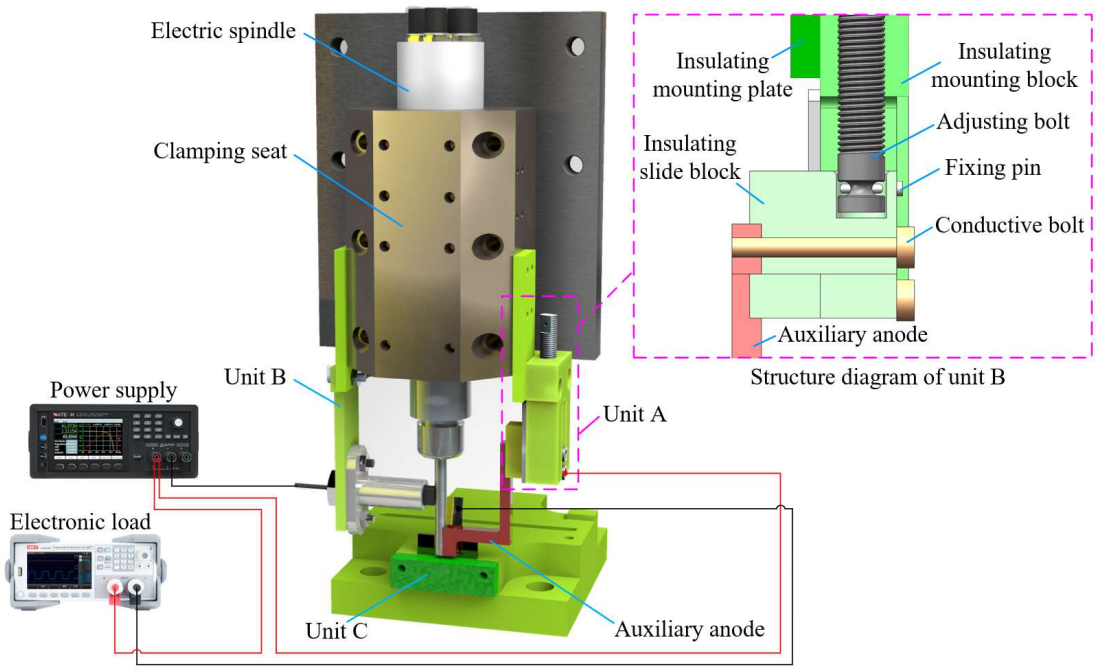


Fig. 4 Schematic diagram of the motor spindle in FAAECMG.

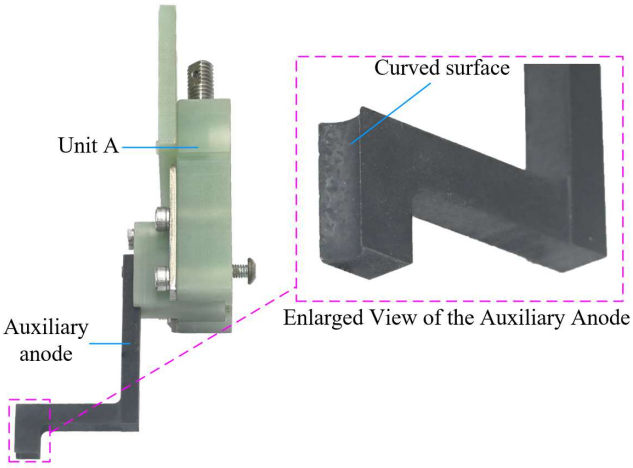


Fig. 5 Photograph of the auxiliary anode and its conductive device.

Table 1 Chemical composition of (TiB+TiC)/Ti-6Al-4V

Element	Ti-6Al-4V	TiB	TiC
Content (vol.%)	94	4.8	1.2

First, efficient removal of a large machining allowance from the (TiB+TiC)/Ti-6Al-4V stepped structure was achieved during the rough machining of ECMG. Subsequently, precision machining was conducted on the machined step surface and its side wall. Both the rough and finish machining stages were performed using a layer-by-layer milling approach [16]. Previous studies have shown that an overcut condition typically occurs during the rough machining stage of ECMG, whereas an overcut-free condition is maintained during the finish machining stag. In earlier work, the authors found that the overcut generated after machining a previous layer during layer-by-layer milling in the rough machining stage can be compensated by increasing the feed amount of the abrasive tool in the subsequent layer. In the present study, the (TiB+TiC)/ Ti-6Al-4V stepped structure was machined in 10 Figlayers during the rough machining stage. The depth of cut of the first layer was 100 μm, the feed amount for the second layer was 200 μm, and the feed amounts for the third to tenth layers ranged from 300 to 350 μm. During the finish machining stage, the feed amount for each layer was set to 10 μm. In addition, the main ECMG process parameters are listed in Table 2. In FAAECMG, ΔU was selected based on the results of the dynamic electric field simulations. To minimize the influence of random errors, each experiment was repeated three times to ensure reproducibility of the results.

Table 2 Main parameters for ECMG

Parameter	Rough machining	Finish machining
Applied voltage	25 V	4 V
Grinding width	6 mm	6 mm
Spindle speed	5000 rpm	10000 rpm
Feed rate	7 mm/min	25 mm/min
Total feed distance	24 mm	24 mm

The machining accuracy of the step surface produced by ECMG was evaluated in terms of surface flatness [23]. Fig. 6 illustrates the measurement method used to determine the surface flatness of the step surface. First, n measurement lines, each with a length of 10 mm, were selected at equal intervals on the step surface. Second, according to Eq. (13), the difference F_i between the maximum height H_{max} and the minimum height H_{min} of the workpiece profile along each measurement line was calculated. Finally, the surface flatness F was calculated using Eq. (14). A smaller value of surface flatness indicates higher machining accuracy. The MRR during the rough machining stage of ECMG was calculated using Eq. (15):

$$F_i = H_{max} - H_{min} \tag{13}$$

$$F=(F_1+F_2+\ldots+F_{n-1}+F_n)/n \tag{14}$$

$$MRR = \Delta M\rho/t \tag{15}$$

where Δm is the mass of material removed, ρ is the density of the workpiece material, and t is the machining time.

Before and after each experiment, the workpiece was weighed using an electronic balance (SQP, Sartorius, Germany) to determine the amount of material removed. The surface profile and surface roughness of the step surface were measured using a confocal microscope (OLS5100, Olympus, Japan). The surface morphology of the step surface was observed using a scanning electron microscope (SEM, Merlin Compact, Germany), and the elemental composition of the step surface was analyzed using energy-dispersive spectroscopy (EDS). The residual stress of the step surface was measured using a residual stress analyzer (XRD, Proto LXRD, Japan).

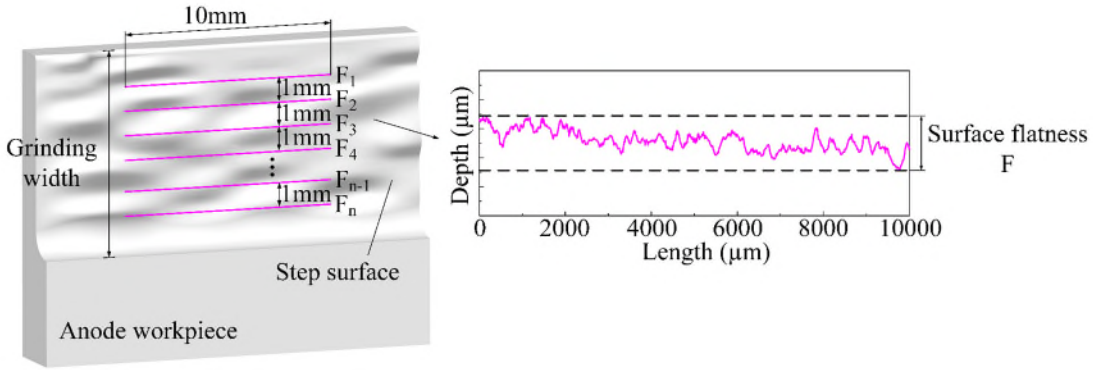


Fig. 6 Schematic diagram of the measurement for surface flatness.

5. Results and discussion

5.1. Electric field analysis

Fig. 7 shows the current density and local electric field line distributions for traditional ECMG and FAAECMG. As shown in Fig. 7(a), in traditional ECMG, the current flows from the machined surface of the workpiece to the working surface of the tool, as well as from the already machined surface of the workpiece to the nonworking surface of the tool, because the potential of the anode workpiece is higher than that of the cathode tool. The current density on the machined surface is relatively high and uniformly distributed. However, as the distance between the already machined surface and the nonworking surface of the tool increases, the current density on the already machined surface decreases. This nonuniform current distribution inevitably leads to stray corrosion on the machined surface, resulting in poor machining accuracy. As shown in Fig. 7(b), in FAAECMG, the auxiliary anode has the highest potential, followed by the anode workpiece, while the tool has the lowest potential. In the machining area, the current flows from the machined surface toward the working surface of the tool. In addition, the current flows from the surface of the auxiliary anode to the machined surface and from the surface of the auxiliary anode to the nonworking surface of the tool. Compared with conventional ECMG, the introduction of an auxiliary anode with a positive potential difference causes a radical change in the current flow direction in the machined area. Because the surface of the auxiliary anode is coated with an inert metal, electrochemical anodic dissolution does not occur on its surface. As a result, stray corrosion on the machined surface is effectively suppressed,

thereby improving process localization.

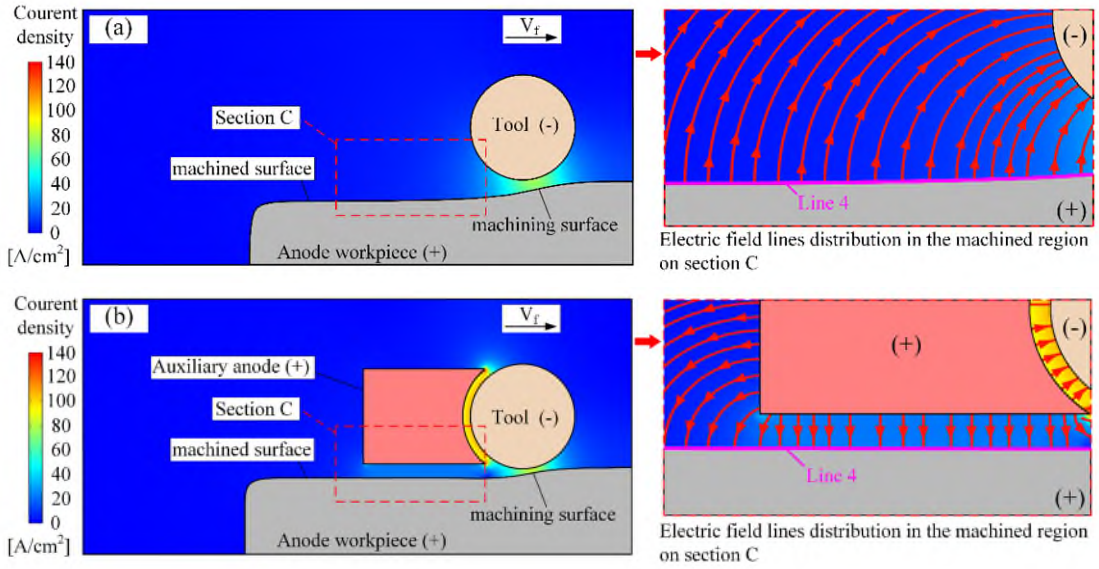


Fig. 7 Electric field line distributions with different machining methods: (a) traditional ECMG, (b) FAAECMG.

The profile of the machined surface along Section C shown in Fig. 7 was defined as Line 4. The surface profile at Line 4 was extracted to calculate the difference in profile coordinates, defined as the depth-direction difference between the maximum and minimum points of the profile. A smaller difference in profile coordinates indicates higher machining accuracy. The profiles of Line 4 under different machining methods and values of ΔU are shown in Fig. 8, and the corresponding differences in profile coordinates are presented in Fig. 9. As shown in the figures, when traditional ECMG was employed, the profile depth of the machined surface increased with increasing distance from the nonworking surface of the tool, resulting in a pronounced arcuate surface profile. Under this condition, the difference in profile coordinates reached 315.59 μm. In contrast, the machined surface became significantly flatter when FAAECMG was applied. When ΔU was 5 V, the difference in profile coordinates decreased from 315.59 μm to 103.76 μm, corresponding to a reduction of 67.12%. As ΔU was further increased to 10 V, 15 V, 20 V, and 25 V, the difference in profile coordinates was reduced by 91.1%, 91.2%, 91.3%, and 91.4%, respectively. These results indicate that once ΔU exceeds 10 V, further improvements in surface flatness become marginal. Conversely, an excessively large ΔU leads to a high potential

difference between the auxiliary anode and the tool, which may induce spark discharge between them.

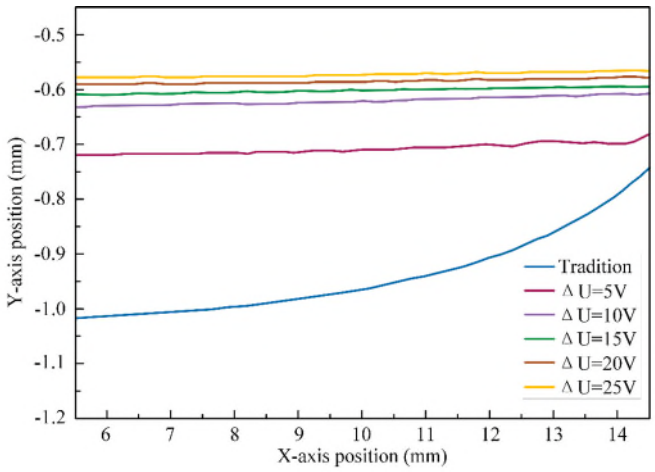


Fig. 8 Profiles of Line 4 under different machining methods and values of ΔU.

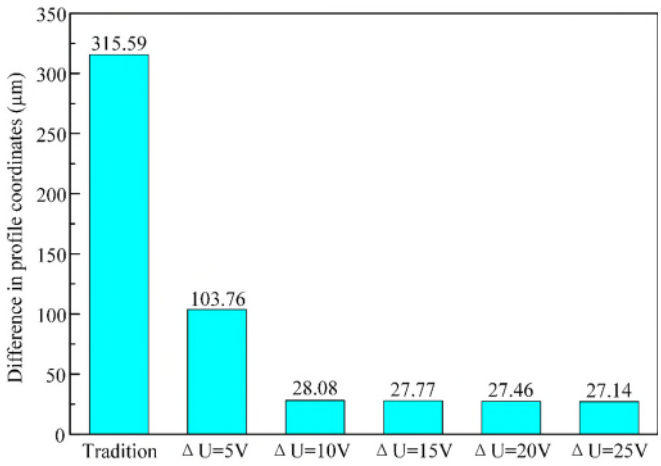


Fig. 9 Differences in profile coordinates of Line 4 under different machining methods and values of ΔU.

5.2. Rough machining of the stepped structure

Fig. 10 compares the surface flatness obtained using conventional ECMG and FAAECMG with different values of ΔU. As shown in the figure, the surface flatness reached 322.5 μm when traditional ECMG was employed. When FAAECMG was applied with ΔU values of 5 V, 10 V, 15 V, 20 V, and 25 V, the surface flatness was reduced to 187.36 μm, 155.79 μm, 152.44 μm, 150.62 μm, and 149.41 μm, respectively. Compared with traditional ECMG, the corresponding reductions in surface flatness was reduced by 41.86%, 51.66%, 52.70%, 53.26%, and 53.64%, respectively. According to the electric field simulation results, stray corrosion on the machined surface was

effectively suppressed by introducing an auxiliary anode with a positive potential difference, thereby enhancing machining accuracy. Consequently, the surface flatness of the step surface was significantly improved when the proposed method was employed. However, when ΔU exceeded 10 V, the reductions in surface flatness between adjacent ΔU values were only 1.04%, 0.56%, and 0.38%, respectively. This indicates that when ΔU reaches 15 V, further increases in ΔU result in negligible improvements in the surface flatness of the step surface.

Fig. 11 further compares the MRR obtained using traditional ECMG and FAAECMG with different values of ΔU. As shown in the figure, compared with traditional ECMG, the MRR decreased by 1.88%, 3.11%, 3.95%, 4.15%, and 4.28%, respectively, when FAAECMG was employed. This reduction in the MRR could be attributed to the suppression of material removal caused by stray currents on the machined surface. However, the improvement in surface flatness was much more pronounced than the reduction in the MRR, indicating that the proposed method has only a minimal impact on the MRR.

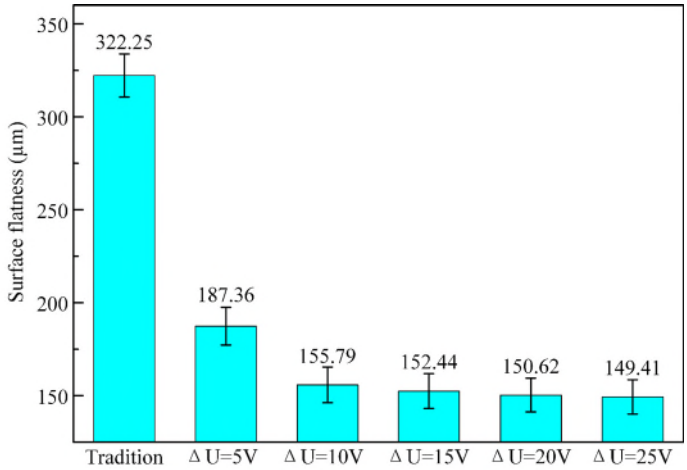


Fig. 10 Surface flatness under different machining methods and values of ΔU.

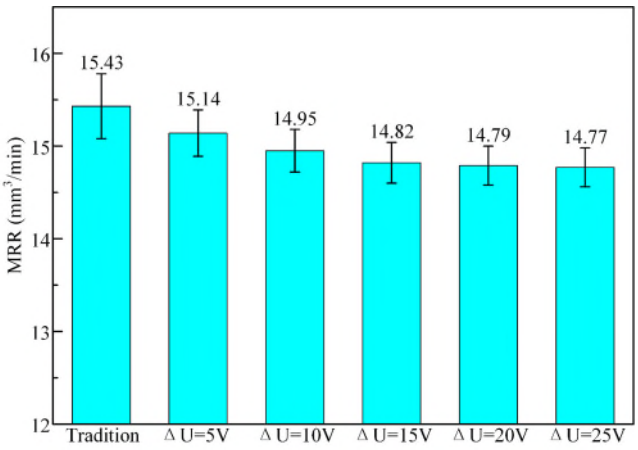


Fig. 11 MRR under different machining methods and values of ΔU.

Fig. 12 shows the stepped structures obtained using traditional ECMG and FAAECMG with ΔU of 15 V. Fig. 13 further presents a comparative analysis of the profiles of the stepped structures along the yellow marked lines L_5 and L_6. As shown in the figures, when traditional ECMG was applied, the step surface profile was uneven, and a pronounced transition fillet formed between the side wall and the nonmachined surface. In contrast, when FAAECMG was applied, the step surface profile became considerably flatter, and the width of the transition fillet between the side wall and the nonmachined surface was significantly reduced. These results indicate that the machining allowance for the step surface and the side wall in the subsequent finish machining stage was significantly reduced when the proposed method is employed.

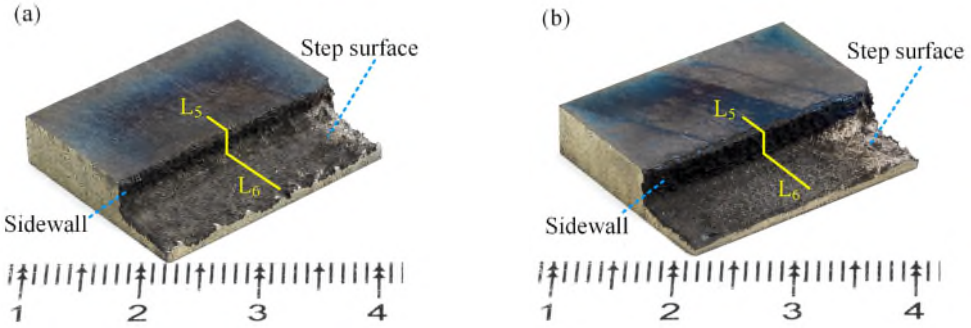


Fig. 12 Stepped structures after rough machining stage: (a) traditional ECMG, (b) FAAECMG with ΔU of 15 V.

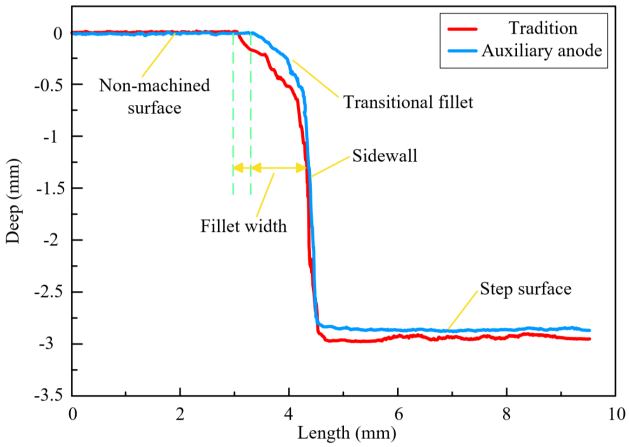


Fig. 13 Profiles of the stepped structure along lines L_5–L_6.

Table 3 compares the machining efficiency and quality achieved using the two methods. As shown in the table, compared with traditional ECMG, the MRR of the stepped structure produced by FAAECMG decreased from 15.43 mm³/min to 14.82 mm³/min, corresponding to a reduction of only 4.15%. In contrast, the surface flatness of the step surface decreased from 322.25 μm to 152.44 μm, representing a reduction of 52.7%, while the surface roughness (Ra) decreased from 16.76 μm to 11.84 μm, corresponding to a decrease of 29.36%. Clearly, the reductions in surface flatness and Ra were significantly greater than the decrease in the MRR when the proposed method was employed. Therefore, FAAECMG could effectively improve the machining accuracy and surface quality of the (TiB+TiC)/Ti-6Al-4V stepped structure during the rough machining stage, thereby contributing to a shortened machining cycle.

Table 3 Machining efficiency and quality under different machining methods

Method	MRR (mm^3/min)	Surface flatness (μm)	Surface roughness (μm)
Traditional ECMG	15.43±0.35	322.25±11.66	16.76±0.52
FAAECMG	14.82±0.22	152.44±9.38	11.84± 0.41

5.3 Finish machining of the stepped structure

Finish machining of the step surface and side wall, following the rough machining stages of both methods, was performed using the parameters listed in Table 2. For the stepped structure produced by traditional ECMG, the number of feeds passes during the finish machining stage was 40 for the step surface and 50 for the side wall, resulting in a total finish machining time of 86.4 min. In contrast, for the stepped structure

produced by FAAECMG, 20 feed passes were required for the step surface and 40 feed passes for the side wall, with a corresponding finish machining time of 7.6 min. The rough machining time was identical for both methods (34.3 min), because the same tool path and feed rate were used. Consequently, the machining cycle for the stepped structure was reduced from 120.7 min to 91.9 min by employing FAAECMG, representing a decrease of 23.86% compared to conventional ECMG. Therefore, these results demonstrate that the newly proposed method can effectively shorten the machining cycle in ECMG of (TiB+TiC)/Ti-6Al-4V stepped structure.

The total material removal volume of the stepped structure during the combined rough and finish machining stages was 476.28 mm^3 when employing the FAAECMG method. Of this, approximately 36.2 mm^3 was removed during the finish machining stage, accounting for 7.6% of the total material removal volume. The stepped structure obtained after the finish machining stage is shown in Fig. 14. The step surface and side wall are flat and smooth, exhibiting a bright metallic luster after the finish machining stage. Vernier caliper measurements show that the width and length of the step surface are 6.4 mm and 24 mm, respectively, while the side wall height is 3.1 mm.

Fig. 15 shows the profiles of the stepped structure at the positions indicated by the yellow lines L_5 and L_6. After finish machining, the step surface profile was flat, side wall profile was steep, and no transitional fillet was observed between the side wall and the nonmachined surface. Compared to the rough machining stage, the surface flatness of the step surface was improved from 152.44 μm to 5.368 μm during the finish machining stage, corresponding to a reduction of 96.48%. These results indicate that the machining accuracy of the (TiB+TiC)/Ti-6Al-4V stepped structure was significantly improved by the finish machining stage.

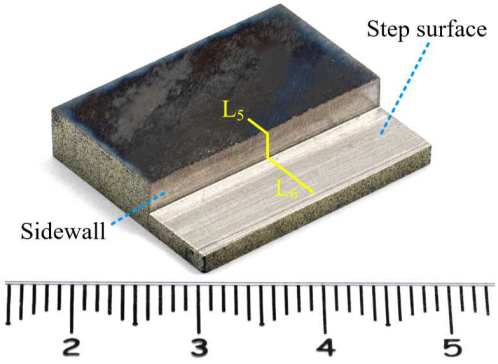


Fig. 14 Stepped structure under finish machining stage.

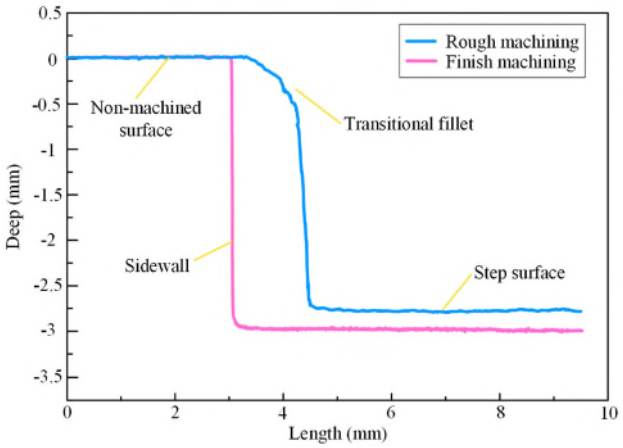


Fig. 15 Profiles of the stepped structure along lines L_5–L_6.

Fig. 16 shows the surface topography and composition of the step surface after rough and finish machining stages. During the rough machining stage, the step surface was uneven, exhibiting an irregular dissolution morphology. In contrast, after finish machining, the step surface was finely and uniformly textured, with no observable pitting or craters.

Compared to the rough machining stage, the contents of O and C elements on the step surface were significantly reduced after finish machining, while the Ti content increased substantially. This indicates that no stray corrosion occurred on the machined surface during the finish machining stage. Fig. 17 shows the surface roughness (Ra) and residual stress of the step surface after rough and finish machining stages. Following the finish machining stage, the surface roughness decreased from 11.84 μm to 0.669 μm, corresponding to a reduction of 94.35%. Meanwhile, the residual compressive stress increases from -116.07 MPa to -407.94 MPa. A smaller surface roughness is known to enhance the corrosion resistance of stepped structure [24].

Moreover, an appropriate increase in residual compressive stress is beneficial for improving fatigue strength [25,26]. These results clearly demonstrate that the surface integrity of the (TiB+TiC)/Ti-6Al-4V stepped structure was significantly improved after the finish machining stage.

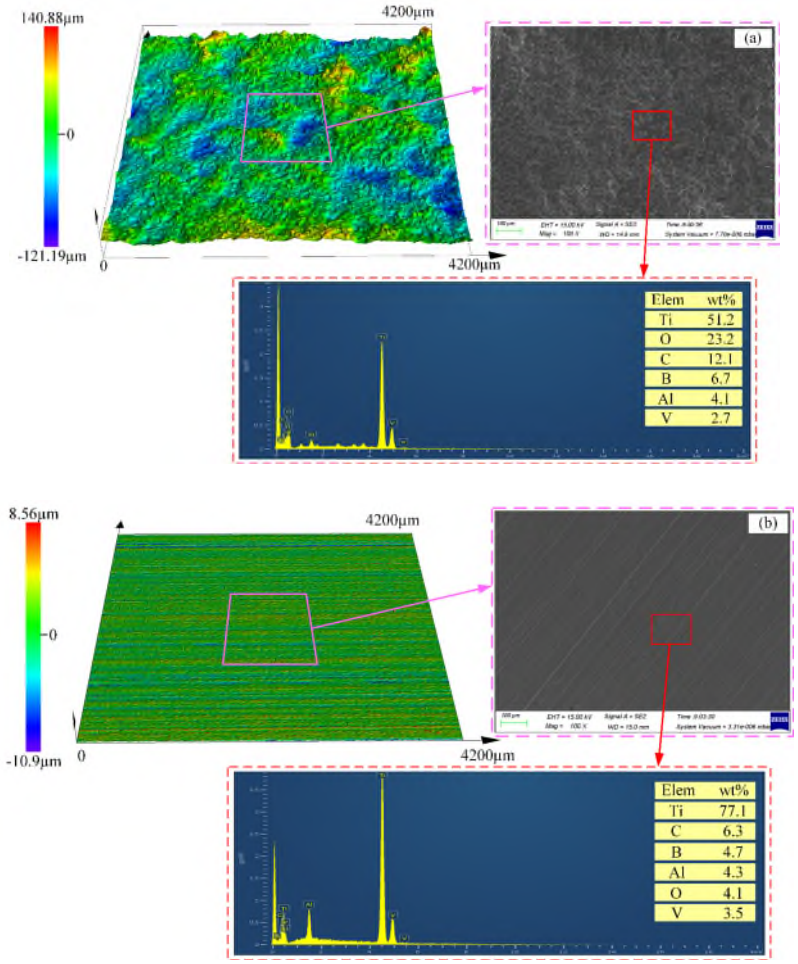


Fig. 16 Surface topography and composition of the step surface after different machining stages: (a) rough machining stage, (b) finish machining stage.

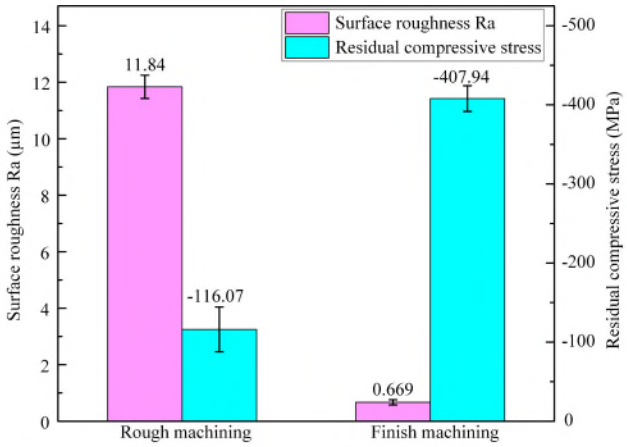


Fig. 17 Surface roughness and residual stress after different machining stages.

In summary, FAAECMG improves the process localization of material dissolution during the rough machining stage, which enhances machining accuracy and surface quality and subsequently shortens overall processing time of (TiB+TiC)/Ti-6Al-4V stepped structure. After rough machining with the proposed method, the machined surface of (TiB+TiC)/Ti-6Al-4V stepped structure was further refined during precise machining without the need to replace the tool or re-fix the workpiece. As a result, (TiB+TiC)/Ti-6Al-4V stepped structure obtained high machining accuracy and good surface integrity after the finish machining stage. Therefore, the newly proposed method can still achieve rough and finish machining in succession. The components made of titanium matrix composites with high machining accuracy and good surface integrity are efficiently accomplished using ECMG by combining the rough and finish machining.

6. Conclusions

In this study, FAAECMG was innovatively proposed for improve machining accuracy and surface quality during the rough machining of titanium matrix composites. A specially designed auxiliary anode with a curved surface was installed behind the abrasive tool using a follow-up conductive device. During the machining process, the auxiliary anode followed behind the abrasive tool at the same feed rate, and its potential was set higher than that of the anode workpiece, thereby suppressing stray corrosion on the machined surface. Based on the dynamic numerical simulation and experimental results, the main conclusions of this study are as follows:

1. The electric field simulation results indicated that introducing an auxiliary anode with a positive potential difference radically altered the current direction in the machined area. This effectively suppressed stray corrosion on the machined surface and significantly reduced the difference in profile coordinates. However, when the positive potential difference exceeded 10 V, the difference in profile coordinates did not continue to decrease obviously, suggesting that further improvement in process localization became insignificant.

2. Compared with traditional ECMG, the decrease in surface flatness of the

(TiB+TiC)/Ti-6Al-4V stepped structure was much greater than the decline in MRR by FAAECMG, resulting in a significant improvement in the machining accuracy of the machined surface. The surface flatness of the step surface no longer decreased dramatically when ΔU reached 15 V. The experimental results validated the reliability of the simulation analysis and confirmed the feasibility of the newly proposed method.

3. Compared with traditional ECMG, when FAAECMG was applied with ΔU of 15 V, the surface flatness of the step surface decreased from 322.25 μm to 152.44 μm, and the surface roughness declined from 16.76 μm to 11.84 μm. Furthermore, the width of the transition fillet between the side wall and the non-machined surface was significantly reduced. The subsequent machining allowance of the step surface and the side wall was considerably reduced using the newly proposed method, thereby shortening the machining cycle of the (TiB+TiC)/Ti-6Al-4V stepped structure.

4. Compared to the rough machining stage, the surface flatness of the step surface decreased from 152.44 μm to 5.368 μm, the surface roughness reduced from 11.84 μm to 0.669 μm, and the residual compressive stress increased from -116.07 MPa to -407.94 MPa after the finish machining stage. Furthermore, stray corrosion on the refined surface was completely eliminated. (TiB+TiC)/Ti-6Al-4V stepped structure with high machining accuracy and good surface integrity is efficiently accomplished using ECMG by combining the rough and finish machining.

Auther contributions Shen Niu: conceptualization, methodology, investigation, experiment, writing-original draft, writing-review and editing. Yansen Peng: investigation, experiment, writing-review and editing. Pingmei Ming: conceptualization, supervision, writing-review and editing. Kaiqiang Huang and Shijie Fan: experiment, writing-review and editing. Wenjie Liu and Lei Ren: supervision, writing-review and editing.

Funding This research was funded by the National Key Research and Development Program of China [No. 2022YFB4601600], the China Postdoctoral Science Foundation [No. 2020M682289], the Key Scientific Research Projects of Henan Provincial Higher Education Institutions [No.26A460009], the Doctoral Foundation of Henan Polytechnic University [No. B2020-30].

Date availability Date are contained within the article.

Declarations

Competing interests The authors declare that they have no known competing financial interests or personal relationships that could have appeared to influence the work reported in this paper.

References

[1] Zhang J, Wang L, Zhao K, Hao Y, Lyu F, Gao Z, Zhao Y, Zhan X (2024) Multiphysics modeling of flow characteristics and particulate migration behavior of titanium matrix composites by laser directed energy deposition. J Manuf Process 131:1014-1029.
https://doi.org/10.1016/j.jmapro.2024.09.062.

[2] Hu Y, Liu Z, Zhang L, Gong S, Wang Z (2025) Enhancing performance in micro-EDM for network microstructure titanium matrix composites utilizing composite pulse power supply. Int J Adv Manuf Technol 141:5563-5580.
https://doi.org/10.1007/s00170-025-16999-2.

[3] Dong G, Guo Z, Cao Y, Lai R, Wu M (2025) Study on chatter stability of TiBw mesh-reinforced titanium matrix composite thin-walled parts in ultrasonic vibration machining. Int J Adv Manuf Technol 137:5877-5898.
https://doi.org/10.1007/s00170-025-15433-x.

[4] Yamada T, Tsuzuku T, Kawachi Y, Yasuhira K (2000) Blade Fabrication Process for Titanium Matrix Composites. Mater Manuf Process 15(3):347-358.
https://doi.org/10.1080/10426910008912992.

[5] Hao X, Zhong P, Li S, Zhang Z, Shu H, Deng W (2024) Process design of one-step deformation to fabricate double-sided gradient structures: Principle, microstructure and mechanical properties. J Manuf Process 132:14-26.
https://doi.org/10.1016/j.jmapro.2024.10.048.

[6] Liu Y, Zhao L, Zhang Z, Huang S, Chen X, Wang Y, Meng L, Zhu H, Xu K, Wang J (2025) Recent progress of advanced sustainable electrolyte jet machining

technologies and its hybrid variants for difficult-to-cut alloy materials. J Alloy Compd 1056.
https://doi.org/10.1016/j.jallcom.2026.186642.
[7] Qu N, Fang X, Zhang J, Kong H, Liu Y, Wang M, Yue X, Ma Z, Shen Z, Chen J (2024) Macro electrochemical milling and its hybrid variants. Chin J Aeronaut 37(8):1-35.
https://doi.org/10.1016/j.cja.2023.12.015.
[8] Yue X, Qu N, Niu S, Li H (2020) Improving the machined bottom surface in electrochemical mill-grinding by adjusting the electrolyte flow field. J Mater Process Technol 276. https://doi.org/10.1016/j.jmatprotec.2019.116413.
[9] Huang S , Ma Q, Liu C, Shi X, Wang C (2022) Research on electrochemical discharge milling of TC4 titanium alloy. Mater Manuf Process 37(16): 1823-1828.
https://doi.org/10.1080/10426914.2022.2065006.
[10] Xue L, Qu N, Ding W (2025) Impact of electrochemical machining parameters on the electrochemical grinding process. Mater Manuf Process 40(5):594-602.
https://doi.org/10.1080/10426914.2025.2462837.
[11] Niu S, Qu N, Yue X, Li H (2019) Effect of tool-sidewall outlet hole design on machining performance in electrochemical mill-grinding of Inconel 718. J Manuf Process 41:10-22. https://doi.org/10.1016/j.jmapro.2019.03.027.
[12] Niu S, Qu N, Li H (2018) Investigation of electrochemical mill-grinding using abrasive tools with bottom insulation. Int J Adv Manuf Tech 97(1-4):1371-1382.
https://doi.org/10.1007/s00170-018-2043-5.
[13] Niu S, Qu N, Yue X, Liu G, Li H (2020) Combined rough and finish machining of Ti-6Al-4V alloy by electrochemical mill-grinding. Mach Sci Technol 24(4):621-637.
https://doi.org/10.1080/10910344.2020.1752236.
[14] Ge Z, Wu Z, Zhu H, Zhu Y (2025) Experimental study on electrochemical grinding of superalloy honeycomb material. Mater. Today Commun 42.
https://doi.org/10.1016/j.mtcomm.2024.111479.
[15] Ge Z, Chen M, Wang R, Zhang B, Zhu Y (2025) Enhancing honeycomb surface quality by harnessing vortex effect in electrochemical grinding. Compos A Appl Sci

Manuf 190.
https://doi.org/10.1016/j.compositesa.2024.108641.
[16] Niu S, Wang H, Ming P, Li D, Wang J, Huang K, Yang G (2025) Effect of Reinforcement Phases on the Electrochemical Behavior of (TiB+TiC)/Ti-6Al-4V Composites in Passivating Solution. JES 172(8).
https://doi.org/10.1149/1945-7111/adfd1e.
[17] Jiang T, Zhu D, Lei G (2025) Electrochemical trepanning with an auxiliary electrode. Chinese J Aeronaut 34(5):183-194.
https://doi.org/10.1016/j.cja.2020.08.041.
[18] Zhang A, Xu Z, Lu J, Wang Y (2020) Improvement of blade platform accuracy in ECM utilizing an auxiliary electrode. Mater Manuf Process 35(9):951-960.
https://doi.org/10.1080/10426914.2020.1752920.
[19] Zhang Q, Luo H, Natsu W (2025) Electrochemical machining mechanism with bipolar pulses and auxiliary electrode elucidated by analyzing behavior of electric double layer. J Mater Process Tech 341.
https://doi.org/10.1016/j.jmatprotec.2025.118907.
[20] Zou Z, Chan K, Wang Y, Huang T, Yue T, Guo Z, Liu J (2024) A new technique for electrochemical self-discharge machining of macro-sized hole in the glass using an integrated tool electrode. J Mater Process Tech 333.
https://doi.org/10.1016/j.jmatprotec.2024.118607.
[21] Jiang T, Zhu D, Lei G (2021) Electrochemical trepanning with an auxiliary electrode. Chinese J Aeronaut 34(5):183-194.
https://doi.org/10.1016/j.cja.2020.08.041.
[22] Yang G, Ming P, Li D, Zeng Y, Zhang A, Qiao H, Niu S (2025) Atomized-electrolyte jet electrochemical grinding for high-precision green machining of hard-to-machine alloys. Chinese J Aeronaut.
https://doi.org/10.1016/j.cja.2025.103977.
[23] Sun C, Xiu S, Zhang P, Li Q, Zou X, Ma L (2022) Influence of the dynamic disc grinding wheel displacement on surface generation. J Manuf Process 75:363-374.
https://doi.org/10.1016/j.jmapro.2022.01.022.

[24] Pramod K, G. S. M, Sumantra M, V S, Kausik C (2021) Enhanced corrosion resistance of the surface modified Ti-13Nb-13Zr alloy by ultrasonic shot peening. Corros. Sci 189.
https://doi.orq/10.1016/i.corsci.2021.109597.
[25] Xiao G, Chen B, Li S, Zhuo X (2022) Fatigue life analysis of aero-engine blades for abrasive belt grinding considering residual stress. Eng Fail Anal 131.
https://doi.org/10.1016/j.engfailanal.2021.105846.
[26] Shen S, Li B, Guo W (2020) Experimental study on grinding-induced residual stress in C-250 maraging steel. Int J Adv Manuf Tech 106(3-4):953-967.
https://doi.org/10.1007/s00170-019-04655-5.